Proceedings World Geothermal Congress 2005
Antalya, Turkey, 24-29 April 2005

The Hall Plot Analysis of a Water Injection Test Affected by Geothermal Reservoir Response

I. Metin Mihcakan,* Elif I. Altinay,* and Ibrahim Kasap**

*Petrol ve Dogal Gaz Müh. Bol., Maden Fak., Istanbul Teknik Univ. Maslak Istanbul 34469, Turkey / mihcakan@itu.edu.tr

**Midas Müh. Müm. Tic. Ltd., Genclik Cad. No. 127-1, Anittepe, Ankara 06570, Turkey

Keywords: Geothermal, Kizildere, Injection Test, Hall Plot Analysis, Reservoir Fill Up, Carbon Dioxide.

ABSTRACT

Water injectivity into geothermal reservoirs is discerned by water injection tests conducted in injection wells and may continue for weeks. The evolution of an injectivity test and the responsive variations in reservoir properties may be ascertained by the steady-state Hall-plot analysis. Thus the efficiency of injectivity may be evaluated by such analysis method, in a continuous manner.

A variable-rate and long-term water injection test, that was conducted in a reinjection well in Kizildere geothermal field, was attempted to be assessed by the Hall plot analysis. The presence of free carbon dioxide gas, prior to the commencement of water injection, is claimed to be detected in the reservoir. At a certain stage in injection operation, the reservoir fill-up and subsequent dissolution of free carbon dioxide in water are also recognized.

1. INTRODUCTION

Various reasons may require the injection of surface waters or the reinjection of produced geothermal waters, which turns out to be disposal water, into geothermal reservoirs, in a continuous manner. Prior to an injection or reinjection operation the water injectivity, i.e., the rate of acceptance of injected water by the reservoir rock, for an injection well is examined by conducting an injection test. Such tests may cover a time span in the order of several weeks or months.

One of the controlling factors that affect the entrance and propagation and, thus, the injectivity of cool injection water into the hot reservoir rock is the resistance exhibited by the formation within few meters around the wellbore. The majority of the force applied to drive injection water into the reservoir rock is used up in this region of resistance. Essentially, the skin effect and the effective permeability to injected water around the wellbore prompt such resistance. In the case of fractures or fissures exist and extend out from the wellbore, the force or energy dissipated for driving the injected fluid in would be much lower in this region.

The difference in temperature of the injected and reservoir waters leads to the propagation of a temperature front in the reservoir, during an injection test. Chemical interactions, induced by temperature differences, between the cool injection water and the hot reservoir rock may cause the precipitation of some of the dissolved mineral species within or without the region of resistance, depending on the advancement of cool water front in the reservoir. Based on the evolution of an injection test, the variations in reservoir properties that may emerge as the reduction in absolute permeability as well as in the effective permeability to cool water may result in a decrease in water injectivity.

Water injectivity is also controlled by the total volume of water that can be injected into a geothermal reservoir and, in turn, is limited with the fracture gradient and the pore volume or liquid storativity of the rock. Once the reservoir is filled with water, the enforcement of more water into the formation leads to a remarkable increase in reservoir and injection pressures, due to the low compressibility of liquid water. The prolonged injection under these conditions will eventually cause the uncontrolled fracturing of the rock or further expanding the existing fractures. Neither of these occurrences is a desired consequence.

Performance analysis and interpretation for water injection operations in geothermal fields may become rather difficult when the injection wellhead pressures and the observation-well bottom-hole pressures are used. Misinterpretations are possible, especially, when the reservoir response to water injection is attempted to be perceived from the monitored injection wellhead pressures or rates in time. Thus, the method of analysis that uses the monitored test data has paramount importance for a reliable evaluation of water injectivity and for the efficient application of the injection operation. The Hall plot analysis is a simple method and is developed to eliminate such difficulties in evaluating the performance of a water injection well.

In this work the Hall plot analysis is applied to evaluate a produced water reinjection test, conducted in KD-1A well in Kizildere geothermal field in Turkey. It is investigated whether the determination of variations in permeability or skin factor could be determined by the Hall plot analysis, as the temperature front propagates during the variable-rate and long-term water injection test. The injection wellhead pressures are used and converted to bottom-hole pressures in the analysis. In the conversion calculations the frictional energy losses and the variation of water density with the change of temperature with depth are taken into account. The recorded pressure and temperature data, of which the latter is recorded at two different depths, at the observation well KD-1, is incorporated in the analysis in order for a better comprehension of the reservoir response.

2. HALL PLOT ANALYSIS

Injection tests employed to determine water injectivity and long-term injection efficiency may last as long as several weeks or months. The transient pressure analysis methods, e.g., falloff tests, injection tests, etc., may not be adequate for evaluating the variations in reservoir characteristics and injection efficiency that occur during the long-term test. Inadequacy is inherent to the essentials of transient pressure analysis methods that estimate reservoir properties at one point in time, whereas the Hall plot is a continuous monitoring method for that purpose (Buell, et.al.1990).

The Hall plot analysis is a steady-state method, originally developed to analyze the water injection well performance in waterflooding applications in oilfields (Hall, 1963). Hall

plot permits monitoring the water injectivity and injection efficiency continuously and provides means to identify the variations in some reservoir properties that occur over the extended period of an injection test (Hall, 1963). Hall plot method has some advantages, such as the smoothing effect on the recorded pressures over time and the use of wellhead pressures, which can be easily converted to bottom-hole pressures using the known techniques.

One of the major difficulties in the analysis of an injection test arises from the variations encountered in the injection wellhead pressures and rates. Such difficulties can be overcome by employing the Hall plot analysis, in which Darcy's law for the steady state flow of single-phase fluids in a well centered in a circular reservoir is used :

$$q = \frac{k_w\, h\,(p_{wf} - p_e)}{18.665\, B_w\, \mu_w\, [Ln(r_e/r_w) + s]} \quad \text{..... (1)}$$

where, "r_e" is the radius extending from wellbore to the front of the cool water bank, i.e., the interface of injected cool water and the hot reservoir water, reservoir pressure at this front, and "p_{wf}" is the bottom hole injection pressure. For a steady-state vertical flow, the bottom-hole pressure can be expressed in terms of wellhead (or tubing head) pressure, p_{tf}, pressure drop due to internal frictional in flow, Δp_f, and fluid head in well, $(\rho g)_w D$, as follows.

$$p_{wf} = p_{tf} + [(\rho g)_w / g_c]\, D - \Delta p_f \quad \text{..... (2)}$$

Although "Δp_f" in Eqn.2 varies with varying injection rate, the magnitude of its variations is at a negligible level. Hall integrated the both sides of Eqn.1 with respect to time :

$$\int_0^t q\, \mathrm{d}t = \frac{k_w\, h}{18.665 B_w\, \mu_w\, [Ln(r_e/r_w) + s]} \int_0^t (p_{wf} - p_e)\, \mathrm{d}t \quad \text{..... (3)}$$

where the left-hand side describes the volume of cumulative water injection, W, and the right hand side gives the total variation in reservoir pressure during the corresponding injection time, t, in days If surface (or wellhead) pressures are desired to be used in practice, then, Eqn.2 is substituted into Eqn.3, and after rearranging Eqn.4 is obtained.

$$\int_0^t \{(p_{tf} - \Delta p_f + [(\rho g)_w\, D / g_c]) - p_e\}\, \mathrm{d}t = m_H\, W \quad \text{..... (4)}$$

where

$$m_H = \frac{18.665 B_w\, \mu_w\, [Ln(r_e/r_w) + s]}{k_w\, h} \quad \text{..... (5)}$$

Note that m_H is the slope of the straight line obtained when the cumulative variation in pressure difference in elapsed time on the left hand side of Eqn.4 is plotted against the cumulative volume of injected water, W. The slope (m_H), although assumed to be constant, increases with increasing radius of expanding cool water front, r_e. The validity of this assumption for constant $Ln\ (r_e/r_w)$ and p_e is explained by Hall (1963), considering the fact that the rate of increase in r_e is constant and independent of changes in skin factor or in effective permeability. As illustrated in **Figure 1**, the slope (m_H) of Hall plot may have misleading values when either wellhead pressures (p_{tf}) or bottom-hole pressures (p_{wf}) are used alone in Hall integral on the left-hand side of Eqn.4. Thus, in order for obtaining a realistic slope and for smoothing the calculated data, Hall integral is suggested to be used in the form of "$\int (p_{wf} - p_e)\, \mathrm{d}t$."

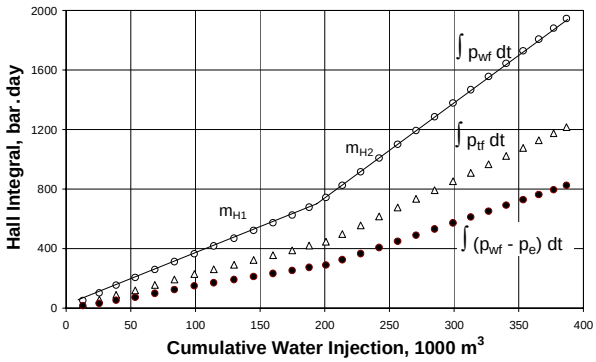

Figure 1 : Comparison of Hall integration methods that differ in slopes in sequential stages of injection.

In all three Hall plots in **Figure 1**, the initial straight-line sections with the slope of "m_{H1}" represent the time interval, in which any variation in effective permeability (k_w) or skin effect (s) has not been encountered yet, during the water injection in a geothermal well. The slopes (m_{H2}) of the second straight-line sections of the curves increase with decreasing "k_w" and increasing "s", as a result of formation damage or any other effect of similar nature. If a stimulation effect takes place during the injection operation, then the slopes (m_{H2}) would decrease with increasing "k_w" and decreasing "s".

Data collection for the Hall plot analysis is inexpensive, since the recording of injection wellhead pressures and rates with respect to time is sufficient. As stated by Buell, et.al. (1990), a major disadvantage of Hall plot analysis is the simultaneous presence of two unknowns, transmissibility (kh/μ) and skin effect (s), in the slope term. The value of transmissibility would change only if a significant change in viscosity or effective permeability occurs. Any change in effective permeability around the wellbore would cause a change in skin effect and, in turn, the slope changes. In this case, the relation between the slopes of two sections on a Hall plot in **Figure 1** may be given as follows.

$$s_2 = s_1 - \frac{k_w\, h}{18.665\, B_w\, \mu_w} (m_{H1} - m_{H2}) \quad \text{..... (6)}$$

where the subscripts "1" and "2" represent the first and second straight-line sections of the plot, respectively. Any formation damage occurred during water injection may be determined by calculating "s_2"in Eqn.6, which requires the value of "s_1" be known from another test, such as falloff, injection or interference test.

If the skin around the injection wellbore is constant and the effective permeability far away from the wellbore changes during water injection operation in a geothermal reservoir, then the transmissibility (or flow efficiency) term for the second straight-line section in Hall plot, in **Figure 1**, can be obtained from the ratio of slopes, as follows.

$$\frac{m_{H1}}{m_{H2}} = \frac{(k_w\, h/\mu_w)_2}{(k_w\, h/\mu_w)_1} \quad \text{..... (7)}$$

The value of $(k_w h/\mu_w)_1$ term for the first straight line is required to be obtained from another test, as in the case of determining skin effect for the second straight line, above.

3. REINJECTION APPLICATION IN WELL KD-1A

Saturated hot water and steam has been produced from two reservoirs in Kizildere geothermal field since 1968. By the mid 1970's, reinjection of waste produced waters back into the upper reservoir was considered, mainly for waste water disposal, supplemental heat extraction, and maintenance of reservoir pressure. A pilot reinjection test was conducted at the well KD-1A, in 1976 (Kasap, 1976), to investigate the water injectivity and injection efficiency. Detailed information on the vindication of reinjection attempt and a general overview of Kizildere geothermal field may be found in elsewhere (Satman, et al, 2000).

During the 29-week long injection operation the average injection rate was approximately 83 tons per hour with ± 10 percent fluctuations, and the injection water temperature varied between 30°C (303 K) and 42°C (315 K),depending on the prevailing test conditions. **Figure 2** illustrates the behavior of wellhead pressure and injection rates, recorded at well KD-1A. The well KD-1, 68 meters away from the injector, was chosen as the observation well and its down-hole temperatures, at the depths of 500 and 530 meters, and bottom-hole pressures were monitored as seen in **Figure 3**. Note that the well KD-1 was drilled to a total depth of 540 meters until a fracture network was encountered where the mud circulation was lost at the depths of 530 to 535 meters.

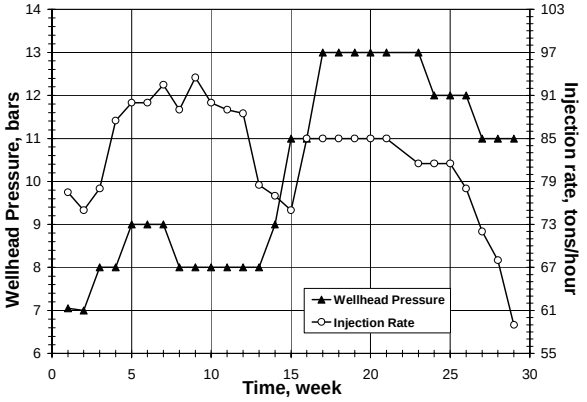

Figure 2 : Variation of wellhead pressure and injection rate with time for the injection well KD-1A.

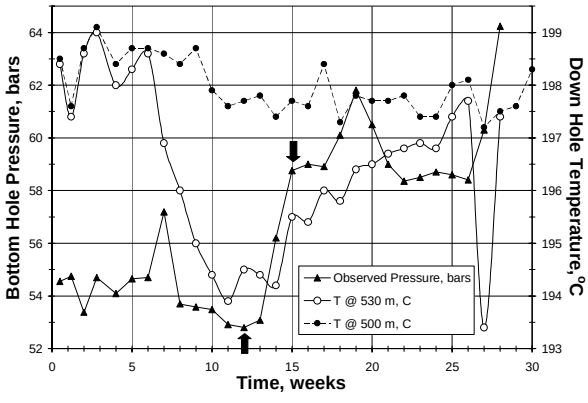

Figure 3 : Down-hole temperatures, at the depths of 500 and 530 meters, and bottom-hole pressures monitored at the observation well KD-1.

As seen in **Figure 2**, in the first 7 weeks, the wellhead pressure increases from 7 bars (0.7 MPa) to 9 bars (0.9 MPa) as the injection rate increases from 75 tons/hr to 90 tons/hr. During the same time frame, both the bottom hole pressure and temperature at 530 meter depth in well KD-1 increase with some oscillations to 57 bars (5.7 MPa) and 198.5°C (472 K), respectively, as seen in **Figure 3**. From 7th to 12th weeks, the injector wellhead pressure drops down to 8 bars (0.8 MPa), and the injection rate oscillates around 90 tons/hr, implying a slight decrease in formation resistance to the injected water around the wellbore and a good hydraulic communication in between the two wells. In other words, no scaling induced permeability reduction occurs about the injector, during this 5-week interval. In the observation well, however, the pressure and temperature at the depth of 530 m drop 4.5 bars and 4.5°C, respectively, yet the temperature at 500-m depth drops only 1°C. Such temperature response at the observation well indicates the arrival of injected water front through the already detected fracture network at the depth of 530 meters in the observer. Therefore, it can be stated that the fracture network does not extend up to the depth of 500 meters and 1°C cooling at this depth is merely due to the conductive heat transfer, while the cooling at the depth of 530 m is due to primarily convective and secondarily conductive heat transfer.

Between the 12th and 15th weeks, injection rate sharply drops from 89 tons/hr to 75 tons/hr, but wellhead pressure increases 3 bars to a level of 11 bars (1.1 MPa), as shown in **Figure 2**. Bottom-hole pressure at the observation well promptly responds to follow a similar trend (**Figure 3**) and increases 6 bars to a level of 59 bars (5.9 MPa). The temperature at 530 m depth at KD-1 increases only 1.5°C by the conductive heating of the rock, since the cooler water flow toward the observation well is mitigated with the rapidly decreasing injection rate. The temperature at 500 m also responds to the alleviated flow of injected water by minor oscillations around 197.7°C.

Tan (1984) attributes such sudden increase in pressure to the plugging up of formation by precipitated silicate (SiO_2), yet, does not provide any explanation for the subsequent increase in injection rate along with the further increase in bottom-hole pressure after the 15th week. Tan's argument for formation permeability reduction as the result of silicate precipitation contradicts with the increase in injection rate. The argument is based only on the observed silicate scaling, with a thickness of 2 to 4 millimeters, on the inner walls of both the surface injection-water flow conduits and wellhead equipment (Kasap 1976). Considerable amount of silicate precipitation out of water in the injection facilities, in fact, leads to the injection of water with low silicate content and, thus, further contradicts with the Tan's argument.

If any solids precipitation took place within the reservoir, then the injector KD-1A would have experienced a pressure rise much earlier than did the observer KD-1. Yet, such response is not seen in Figures 2 and 3. Consequently, the injection rate and pressure behavior between 12th and 15th weeks should actually be considered as a good example for the reservoir fill up by injected water. It is known that the long term depletion of lower reservoir caused the formation and the subsequent vertical migration of a free gas phase, consisting of essentially carbon dioxide and some water vapor, into the upper reservoir in Kizildere field. After the arrival of injected water at the observation well, on the 6th week of operation, it is more likely that the further injection is filling up the reservoir while compressing the free gas phase. The sharp increase in bottom-hole pressure, shown in between the solid arrows in **Figure 3**, may be attributed to the dispersion of free gas phase in liquid water upon compression. Simultaneously the decline in injection rate is lessened (**Figure 2**) as the volume of dispersed gas phase is replaced by slowly increasing volume of water. Since the cool injection water fills up the reservoir at a low rate and

warms up, the temperature at 530-m depth increases with oscillations, and the temperature at 500-m depth around well KD-1levels off, as seen in **Figure 3**. The reservoir fill up seems to be completed by the end of 15th week.

After the 15th week, the injection rate increases about 10 tons/hr and remains constant at the level of 85 tons/hr. The wellhead pressure follows the same trend with one week delay, then increases 2 bars and remains constant at 13 bars (1.3 MPa), until the 21st week., as in **Figure 2**. The bottom hole pressure at the observation well responds to the rate increase with two-week delay and rapidly rises up to a peak of about 61.7 bars and, then, rapidly drops down to 58.2 bars, until the 22nd week, as shown in **Figure 3**.

According to the authors of this paper, such pressure and rate behavior resembles either the enlargement of existing fractures or a small scale fracturing in an already pressured up formation. It is well known that once the fracturing is started, its propagation does not require as much pressure as for initiating the fracture. Bottom-hole pressure behavior, between the 17th and 22nd weeks in **Figure 3**, seems to be an indicator for such occurrence, which may be interpreted as the compression of injected excessive water until the start of fracturing or fracture enlargement on the 19th week. Within the same time frame, the injection wellhead pressure in **Figure 2** rises up to the highest level of 13 bars and remains constant. Probably the fracture enhancement was not so extensive to relax the system and to cause a drop in wellhead pressure. In the mean time, both temperature responses at the depths of 500 and 530 meters (**Figure 3**) support this interpretation by maintaining their behavior with minor oscillations between the 15th and 22nd weeks.

After the 22nd week, both the injection rate and wellhead pressure begin to decline (**Figure 2**) and the bottom hole pressure starts rising, since the reservoir is already filled up and does not accept additional water below the gradient for generating new and substantial fractures. Eventually, the reinjection operation was stopped at the end of 29th week.

4. EVALUATION OF TEST PRESSURE DATA

The pressure data recorded at the injection and observation wells are evaluated in order to estimate several reservoir properties and to apply Hall plot analysis on the injection test. Initially the wellhead pressures, p_{tf}, are converted to bottom-hole pressures, p_{wf}, according to Eqn.2, so that the Hall integral in "$\int (p_{wf} - p_e)\,dt$"form could be evaluated.

4.1 Calculation of Injection Bottom-Hole Pressures

For calculating the bottom-hole pressure at each injection rate, the wellbore is divided into 12 imaginary sections with equal section height of 45 m, except the last section. Last section has the height (or depth interval) of 35 m. The density, temperature, frictional pressure losses, and pressure of water are calculated iteratively for the bottom of each section. Since the injection water has rather low TDS of approximately 5000 ppm, density calculations are based on ordinary water assumption. Water densities at prevailing temperatures, between 20°C and 200°C, and at pressures, between 1 bar and 60 bars, are determined using the data extracted from the Steam Tables in SI Units (1990). The extracted data is plotted as in **Figure 4**, for practical use. More accurate estimation of density is obtained using the following equation, which is fitted by linear regression to the plotted data in **Figure 4** (Altinay, 2002).

$$\rho = C1\,p^5 + C2\,p^4 + C3\,p^3 + C4\,p^2 + C5\,p + C6 \quad \text{..... (8)}$$

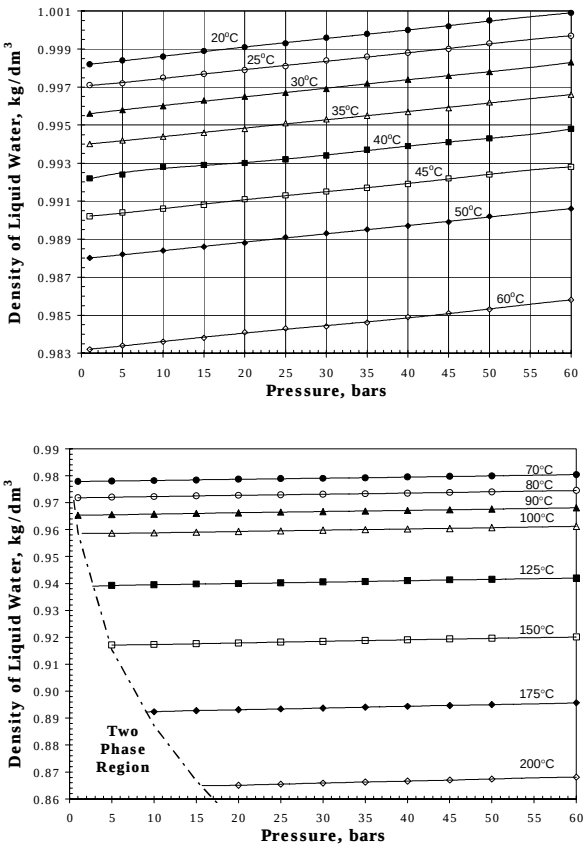

Figure 4 : Density of liquid water plotted as a function pressure and various temperatures, using the data from Steam Tables in SI Units (1990).

In Eqn.8, the density (ρ) at a particular temperature is in kg/dm^3 and is dependent on pressure (p) in bars. Constants of A to F are the regression coefficients, tabulated in **Table 1**, and are to be multiplied by the number in parenthesis just below the title of that particular constant at the top of the its pertinent column. Iteratively calculated water density in each section is used to estimate both the frictional pressure losses and the bottom pressure for the particular section.

Table 1 : Density of liquid water plotted as a function pressure and various temperatures, using the data from Steam Tables in SI Units (1990).

T (°C)	C1 ($\times 10^{-12}$)	C2 ($\times 10^{-9}$)	C3 ($\times 10^{-8}$)	C4 ($\times 10^{-6}$)	C5 ($\times 10^{-5}$)	C6 ($\times 10^{-1}$)
20	-6.8052	1.0273	-5.4310	1.1412	3.8972	9.9817
25	-7.8467	1.,1825	-6.3649	1.4768	3.0909	9.9706
30	6.8655	0.97455	4.9347	-1.1101	5.6449	9.9554
35	-3.6339	0.57126	-3.2046	0.76921	3.6726	9.9398
40	3.0852	-5.0725	30.336	-7.8416	11.992	9.9205
45	-1.2932	1.8709	-9.4205	1.9218	3.0993	9.9018
50	-3.6339	0.57126	-3.2046	0.76921	3.6726	9.8798
60	-9.9320	1.4686	-7.1927	1.2804	3.7427	9.8317
70	-9.9320	1.4686	-7.1927	1.2804	3.7427	9.7777
80	-1.3046	1.8938	-9.1132	1.5874	3.8424	9.7176
90	-1.0922	1.8514	-10.831	2.5111	2.7938	9.6528
100	-1.5633	2.8329	-18.674	5.4317	-1.9372	9.5859
125	2.7342	-4.6916	29.343	-8.0664	14.246	9.3865
150	-1.7798	2.9962	-19.035	5.5479	-1.3290	9.1705
175	5.6712	-9.7354	62.738	-18.782	32.258	8.9052
200	-13.597	25.831	-188.84	66.135	-102.99	8.7065

As seen in Figure 4, the density of injected water is a function of its pressure and temperature. It is a known fact that the temperature of injection water varies along the well depth, as a result of thermal energy exchange between the earth and water in the well. Thus, the following equation proposed by Ramey (1962) is used to calculate an average water temperature for each imaginary section in the well.

$$T_i\,(z.t) = a\,z + b - a\,A + \left[T_0\,(t) + a\,A - b\right] e^{-z/A} \quad \text{..... (9)}$$

where T_i is the temperature of injection water in °C at depth z and time t, T_0 is the wellhead temperature of injection water in °C, t is the time since the start of injection, a is the local geothermal gradient in °C/m, A is the time function, b is the geothermal surface temperature in °C, and z is the depth from the top of each section in meters. Here the time function, A, is defined as (Ramey, 1962),

$$A = \frac{q_m\ c_p\ \left[\lambda_e + r_{pi}\ U\ f(t)\right]}{2\,\pi\ r_{pi}\ U\ \lambda_e} \quad \text{..... (10)}$$

where q_m is the injection mass flow rate in kg/d, c_p is the specific heat of water at constant pressure in J/kg °C, λ_e is the thermal conductivity of earth in W/m °C, and r_{pi} is the inner radius of injection pipe in meters. The dimensionless transient heat transfer function for earth, $f\,(t)$, is estimated using the following expression.

$$f(t) = -\,Ln\left(\frac{r_{po}}{2\sqrt{\alpha\,t}}\right) - 0.290 \quad \text{..... (11)}$$

where r_{po} is the outer radius of injection pipe in meters, α is the thermal diffusion coefficient of earth in m^2/d, and t is the time elapsed since the start of injection. The overall heat transfer coefficient, U, in W/m^2 °C per unit depth in Eqn.11 is determined from

$$\frac{1}{U} = \frac{1}{2\,\pi}\left[\frac{1}{h_w\ r_{pi}} + \frac{Ln\,(r_{po}\,/\,r_{pi})}{\lambda_p} + \frac{Ln\,(r_{co}\,/\,r_{ci})}{\lambda_c}\right] \quad \text{..... (12)}$$

where r_{pi} and r_{po} are the inner and outer radii of injection pipe, and similarly r_{ci} and r_{co} are the inner and outer radii of cement, respectively. Thermal conductivity coefficients for the injection pipe and cement are designated as λ_p and λ_c and are selected as 43.3 and 0.865 W/m °C, respectively. Since the silicate precipitation in surface flow lines was significant, the silicate scaling on the injection pipe walls is thought to be negligible and, thus, omitted in the calculation of overall heat transfer coefficient, U.

The thermal convection (film) coefficient of water, h_w, is estimated in W/m^2 °C for each imaginary section in the well using the Dittus-Boulter equation (Çengel, 1998).

$$Nu = 0.023\,Re^{0.8}\ Pr^{n} = \frac{2\,r_{pi}\ h_w}{\lambda} \quad \text{..... (13)}$$

where the Nusselt number, Nu, is calculated using the Prandtl number, Pr, of 4.87, and the Reynolds number, Re, which is iteratively calculated for each flow rate and water density in the particular well section. Note that the power "n" of the Prandtl number is 0.4 for heating and is 0.3 for cooling of flowing water. Obtained Nu values are used to estimate "h_w" for the λ = 0.618 W/m °C of water. As seen in **Figure 5**, the point values of h_w decrease slightly, as water cools down by loosing thermal energy to the cooler surroundings until the depth of 135 meters, and increases non-linearly as water heats up by gaining thermal energy from the earth, below that depth. **Figure 5** also implies that the higher the injection rate the greater the thermal film convection coefficient of water, h_w, without a remarkable change in its depth dependent profile.

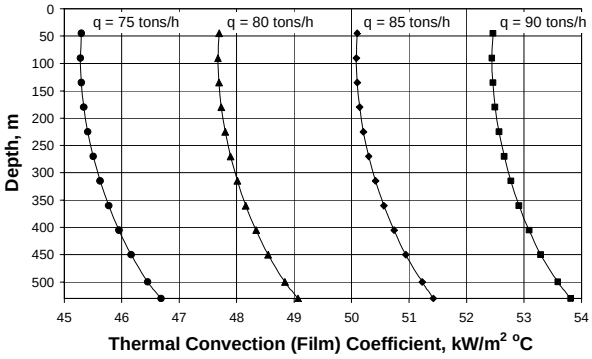

Figure 5 : Variation of thermal convection coefficient, h_w, of injection water with well depth.

For the minimum and maximum injection rates Re is found to be varying between 16.4×10^4 and 20.5×10^4. Since the Reynolds number, Re, is a function of water density, which varies with temperature and pressure, Eqn.2 and Equations 8 through 13 are solved consecutively by iterating on density, temperature and pressure. Iterations are continued until the calculated temperature, density, and pressure of injected water at the bottom of each imaginary section did not change beyond the selected margins of error.

The change in water density, ρ, along the well for various injection rates (q) and wellhead pressures (p_{tf}) is shown in **Figure 6**. As expected, for the same wellhead pressure the higher the injection rate the higher the density of injected water. Similarly, for the same injection rate the greater the wellhead pressure the higher the injected water density. It seems that the wellhead pressure has more effect than the injection rate on the injected water density, particularly in the lower or deeper parts of the well.

Despite the continuous increase in pressure in sequential well sections, water density increases to the depth of about 350 m and, then, decreases to the depth of 530 m. Such density behavior implies that, below the depth of about 350 meters, the volumetric expansion of water due to its thermal energy gain from earth is greater than the volumetric compression of the same water by the fluid head above.

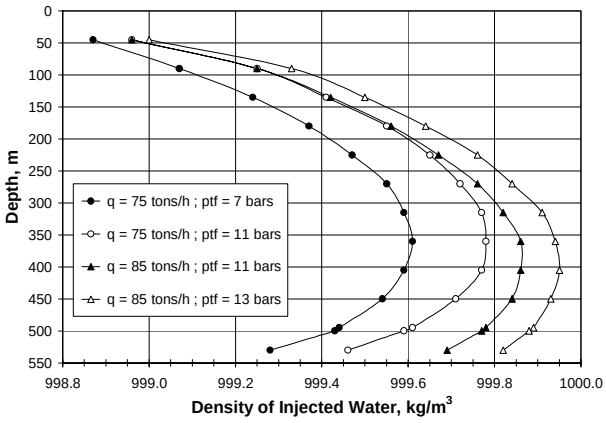

Figure 6 : Changes in water density with well depth for various injection rates and wellhead pressures.

Once the injection water density is determined in a section, the head of water for that section is calculated and added on to the section top pressure to obtain the section bottom pressure. The same calculation steps are repeated for each section, until the bottom-hole injection pressure is obtained. The gravitational acceleration of earth, g, is determined to be 9.7902 m/s^2 (CRC, 1991) for Kizildere field, which is about 180 m above sea level at the latitude of 37° 53' and the longitude of 28° 23'. Thus the ratio of "g/g_c" in Eqn.2 is determined to be 0.9983.

Upon the determination of variation of water density with depth the frictional pressure loss, Δp_f, in each section is estimated using modified Darcy-Weisbach formula,

$$\Delta p_f = 1.9167\times10^{-7}\,\frac{f\,L}{r_{pi}^5}\,\frac{q_m^2}{\rho\, g_c} \quad \text{..... (14)}$$

in where f is the Moody friction factor obtained iteratively from Colebrook equation, L is the section length in meters, ρ is the density of water in kg/m^3, g_c is the conversion factor of 9.806 kg_m m/s^2 kg_f. Eqn.14 is modified in the sense that it is derived for mass flow rate, q_m, in tons/h and its coefficient is specific for the Kizildere field.

The injection water temperature at the wellhead, although varies between 20°C and 42°C during the test, is assumed to be constant at an average value of 35°C. It is found that such variation in moderate injection water temperature has a negligible effect on the calculated bottom-hole injection pressures, particularly at shallow depths. For instance, at the depth of 530 meters, the pressure of water at 20°C is only 0.3 bars greater than that of at 40°C. Should the error in pressure measurements, committed by using the conventional gauges at the time of injection in 1976, is considered, it would be conceivable that less than 0.2 bar difference in bottom hole pressure calculations is very minor and, for all practical purposes, does not affect the results. For greater injection depths, the variations in injection water temperature should be taken into account in the bottom-hole injection pressure calculations.

4.2 Estimation of Average Reservoir Pressure

Average reservoir pressure around the injection well prior to the injection operation is estimated to be approximately 54.5 bars at 530-meter depth. The estimated pressure is calculated based on the reservoir pressure of 46.2 bars, observed at the depth of 430 meters before injection. The density of reservoir water used in calculations is estimated as 872.7 kg/m^3 for the TDS of 5000 ppm and the steam fraction of 11 percent at surface pressure and temperature (Ugur, 1996).

As seen in **Figure 3**, the bottom-hole pressure at the KD-1 observation well had been fluctuating around 54 bars, early in the operation. This observation well pressure, recorded before the effect of injected water was felt, confirms the average reservoir pressure estimated at the injection well.

5. HALL PLOT ANALYSIS OF REINJECTION TEST

The Hall plot analysis is applied using Eqn.4 to evaluate the reinjection test conducted in well KD-1A. Bottom-hole pressures that are converted from wellhead pressures are employed in the analysis. As shown in **Figure 7**, the values of Hall integral in "bar·day" are plotted against the volume of cumulative water injection in 1000 m^3. The Hall plot exhibits two straight lines, of which the second line deviates from the first line after the 12th week of injection.

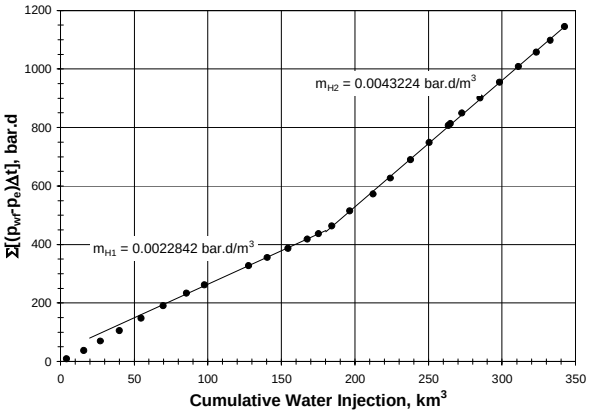

Figure 7 : Hall plot for the Well KD-1A reinjection test.

The slopes of the first and second straight lines, indicated by solid circles, are determined to be m_{H1} = 0.0022842 and m_{H2} = 0.0043224, both are in bar·day, respectively. The slope of the second line being almost twice that of the first line may be interpreted as the increase in skin value, from s_1 to s_2, after the 13th week of injection, when Eqn.6 is considered. The other interpretation may be the decrease in permeability, from k_{w1} to k_{w2}, if Eqn.7 is considered. Either occurrence is possible to take place in-situ when the solids precipitate as the mixing zone of the injected and reservoir waters move away from the wellbore. However, the rate, pressure, and temperature observations at both wells do not indicate such formation damage, until the end of the 13th week of injection, as explained in section 3 above.

5.1 Determination of Reservoir Properties

In order to have an idea about the transmissibility, kh/μ, between the two wells, a simple interference test analysis is performed using the injection rates and observation well pressures recorded until the injected water arrives at the observation well KD-1 on the seventh week. Decrease in pressures due to the cooling effect of injection within that period is ignored and the type-curve matching technique is applied in the interference test analysis (Earlougher, 1977). The transmissibility, kh/μ, between wells KD-1A and KD-1 is determined as 5028.3 mD·m/mPa·s.

A skin factor of $s_1 = -5.85$ is calculated by substituting the estimated transmissibility in Eqn 5, for first straight line behavior in **Figure 7**. Such a low skin factor is regarded as the confirmation of a fracture network exists around the observation well. Note that a fracture network was detected by a remarkable mud loss when the bottom part (535-540 meter interval) of KD-1 was drilled. The fracture network is presumed to extend to the injection well, because the apparent wellbore radius, r_{wa}, calculated by Eqn.15 for the injection well is found to be 39 meters and seems to support this presumption.

$$r_{wa} = r_w\, e^{-s} \quad \text{..... (15)}$$

Satman (1988) also hypothesizes the existence of a fracture network of 12 fractures around the injection well, based on the results of heat-flow model calculations. Consequently, it is decided that a fracture network is extending from well KD-1A to KD-1 within the depth interval of 530-540 m and is acting as an efficient flow conduit.

The skin factor, s_2, for the second straight line behavior in **Figure 7** is calculated using Eqn.6 and found as "– 5.35". Since both skin factors are not very different from each

other, it can be stated that the reinjection operation has not caused a significant mineral precipitation induced plugging of fractures in the formation. The latter skin factor is used in Eqn.15 to evaluate the change in the apparent wellbore radius and found as 24 meters, implying a minor plugging (if there is any) in the formation.

Type-curve matching parameters of the interference test analysis are further used to estimate the reservoir storativity as $\phi h c_t$ = 0.0958 m·bar^{-1}. Since the effective formation thickness (h), through which the injected water flows, is unknown, neither the effective permeability (k_w) nor the porosity (ϕ) within the fractured system can be estimated.

5.2 Analysis of Reservoir Fill-Up

Though the combined results of Hall plot and interference test analyses indicate a minor damage in reservoir, the rate, pressure, and temperature responses at both wells do not support such thesis. It is clear from **Figure 3** that the injected water breakthrough at the observation well occurs after the injection of 85,565 m^3 of water as of the 7th week. Then, cooling and subsequent pressure decline takes place around the observation well until the 12th week, during which an additional 82,116 m^3 of water is injected. If there were a significant mineral precipitation induced plugging in the reservoir, injected water breakthrough and subsequent cooling would not have occurred in those 12 weeks. Even if significant plugging had occurred, the injection wellhead pressure would be expected to rise slightly, instead of staying constant at 8 bars, as seen in **Figure 2**. Thus, the pressure, rate, and temperature behavior observed in both wells is attributed to the filling up of the reservoir between the 7th and 12th weeks.

Existence of free carbon dioxide (CO_2) with water in the upper reservoir was detected when the wells completed in the upper reservoir produced free CO_2 gas. Therefore, until the end of 12th week, free CO_2 gas had to be somewhat compressed and some of it had to be dissolved in injected water, as the liquid-vapor system tried to reach equilibrium. In the mean time, continuous heating up of the injected water must have affected the progress of CO_2 dissolution or liberation in the course to the observation well. As the reservoir is filled up the injection rate decreases but the injection pressure stays constant, as the cooling comes to an end and pressure starts rising around the observation well.

As marked by the solid arrows in **Figure 3**, between the 12th and 15th weeks the pressure at both wells rise sharply but the temperature around the observation well increases with oscillations. Such reservoir response is attributed to the reservoir fill up so that the injected additional water is no more flowing with ease towards the observation well but forcing the free CO_2 to dissolve in water. In other words, the injection of 28,745 m^3 of water, between 12th and 15th weeks, starts raising the free water level (or the liquid water saturation) in the reservoir as the free CO_2 gas is forced to be dispersed in water.

At this point a compressibility calculation is performed to evaluate whether the sharp increase in pressure was the reflection of the compression of free CO_2. The changes in volume and pressure between the solid arrows in **Figure 3** are used and the compressibility of free CO_2 is calculated to be c_{cd} =2.48 × 10^{-2} bar^{-1} at approximately 195°C. Satman and Ugur (2002) declared c_{cd} =2.49 × 10^{-2} bar^{-1} at 200°C. Such result is considered as a good evidence for the fill up scenario hypothesized in this study, yet a material balance calculation is attempted for further support of this scenario.

5.3 Material Balance Calculations

If there were free CO_2 phase within the fracture network, before its complete dispersion in water prior to the 16th week, then, estimating the saturations of both water and CO_2 phases at the time of breakthrough should be possible. The injected volumes of water during the 3 sequential injection stages of 1st to 7th week, 7th to 12th week, and 12th to 15th week are used in a material balance calculation for this purpose.

In the third stage, between the 12th to 15th weeks, the volume of injected water, $V_{12\text{-}15}$ = 28,745 m^3, should be equal to the volume of compressed and dispersed CO_2 in water. In the second stage, between the 7th to 12th weeks, the volume of injected water, $V_{7\text{-}12}$ = 82,116 m^3, should be equal to the volume of expanded CO_2 due to cooling effect of injected water. The sum of these volumes should yield the volume of free CO_2 in the reservoir, V_{cd} = 110,861 m^3, at the time of breakthrough on the 7th week. The volume of water injected until the breakthrough, V_w, is 85.565 m^3. Thus, at the time of breakthrough, the saturations of water and free CO_2 phases are calculated from,

$$S_w = \frac{V_w}{V_w + V_{cd}} \quad \text{..... (16-a)}$$

$$S_{cd} = \frac{V_{cd}}{V_w + V_{cd}} \quad \text{..... (16-b)}$$

and water and CO_2 saturations around the observation well are obtained as S_w = 0.436 and S_{cd} = 0.564, respectively. Using these saturations the total compressibility of the fluid system, c_t, is estimated from the expression of

$$c_t = S_w\, c_w + S_{cd}\, c_{cd} + c_f \quad \text{..... (17)}$$

where the formation compressibility, c_f, is ignored since its magnitude is insignificant compared to that of the water and free CO_2 compressibility. The compressibility of Kizildere reservoir water is determined to be c_w =2.648 × 10^{-2} bar^{-1} at the breakthrough temperature of 197°C (Satman and Ugur, 2002). Note that the Kizildere reservoir waters with a TDS of 5000 ppm contain only about 1.5 percent dissolved CO_2. As a result the total system compressibility is estimated as c_t = 1.681 × 10^{-2} bar^{-1} at the time of breakthrough.

Substituting the total compressibility in the storativity, $\phi h c_t$, of 0.0958 m·bar^{-1}, obtained by the interference test analysis, yields ϕh = 5.7 m. The product of ϕh is for the fracture network, through which the injected water and CO_2 gas flows. Since the distance, r_{bt}, traveled by the injected water until breakthrough, for a radial system, can be expressed as

$$r_{bt} = \sqrt{\frac{V_w\, B_w}{\pi\, \phi\, h}} \quad \text{..... (18)}$$

Solving Eqn.18 results in r_{bt} = 72 meters, which is only 4 meters different than the surface distance between the wells KD-1A and KD-1. Thus, the results obtained by material balance application seem to be acceptable and confirming the reservoir fill up, considering the lack of information on the actual distance and the geometry of fracture network between the two wells at the depth of 530 to 540 meters.

Consequently, the slope change in Hall plot here indicates essentially the resistance to flow caused by the reservoir fill up. Even if there were any formation damage, it was minor and could not be detected from Hall plot in this case.

5.4 Fracture Enhancement

As was discussed previously in Section 3, the start of a short-term increase in injection rate and a rapid but finite increase in injection pressure after the 15th week is thought to reflect either an enlargement of existing fracture network or a small scale hydraulic fracturing in the already filled up formation (**Figure 2**). The rapid increase and subsequent rapid drop in observation well pressure after the 16th week, in **Figure 3**, supports such interpretation. Normally the effect of such fracture enhancement is expected to be seen as a decrease in slope in the Hall plot, starting from the 21st week or after the cumulative water injection of 250,000 m^3.

If **Figure 7** is carefully inspected, although very slight, a decrease in slope may be seen. Yet such claim would be speculative, if the compressibility of water with high CO_2 content, the assumption of constant reservoir pressure in Hall integral, and the error in pressure measurements are taken into account. Thus, it can be stated that the limited but rapid increase in injection rate, prior to the rapid jump in observation well pressure, reflects a minor enhancement or fracturing in the fracture system around the observation well. The fracture enhancement must be rather minor, so that it did not cause a distinct change in the Hall plot slope.

6. CONCLUSIONS

Hall plot analysis is applied to a reinjection test conducted in well KD-1A in Kizildere geothermal field to investigate the possible changes in reservoir properties. The change in slopes of Hall-plot straight lines alone implies damage in the reservoir. However, incorporating the pressures and temperatures, monitored at the observation well KD-1, in interpretation indicates reservoir fill up with the injected water. An interference test analysis, performed by using the injection rates and observation well pressures, provides means to quantify the transmissibility and storativity of reservoir. The results of material balance calculations, when combined with that of the interference test and Hall plot analyses, reveals that the reservoir fill up caused the slope change in the Hall plot and masked the variation, if there were any, in reservoir properties. Interpretations also confirm the previously detected presence of free carbon dioxide gas phase within the fracture network in reservoir.

1. Hall plot analysis can be used to evaluate the injection performance, reservoir properties, and reservoir response in long term water injection tests applied in geothermal wells, with the requirement of at least reservoir transmissibility and storativity obtained from another type of test, such as an interference test.

2. Reservoir fill up, which should occur in a long term injection test, may mask the possible variations in reservoir rock properties and, thus, may lead to misleading interpretations if the Hall plot analysis results are used alone.

3. Hall plot and interference test analyses together may help detecting the fracture network, if essentially all fluids in the system saturate and flow through the fracture system.

4. A minor fracture enhancement cannot be detected by Hall plot, unless the fracture enhancement causes a distinct decrease in the slope of Hall plot.

5. In the conversion of injection wellhead pressures into the bottom-hole pressures, the variations in injection water density ought to be determined by taking the salinity and the increasing temperature and fluid head into account. Particularly in wells deeper than 600 meters, the accurate estimation of injection water density can make significant difference in calculated bottom-hole pressures.

NOMENCLATURE

A : time function, m
a : local geothermal gradient, °C/m
B_w : formation volume factor of water, m^3/sm^3
b : geothermal surface temperature, °C
c_{cd} : compressibility of carbon dioxide, bar^{-1}
c_f : compressibility of formation, bar^{-1}
c_p : specific heat of water at constant pressure, J/kg °C
c_t : total compressibility, bar^{-1}
c_w : compressibility of reservoir water, bar^{-1}
f : Moody friction factor, dimensionless
$f(t)$: earth transient heat-transfer function, dimensionless
h : reservoir thickness, m
h_w : thermal convection coefficient of water, W/m^2 °C
L : flow distance, m
m_H : straight line slope in Hall plot, bar·d/m^3
Nu : Nusselt number, dimensionless
Pr : Prandtl number, dimensionless
p_{obs} : observation well bottom-hole pressure, bar
p_{tf} : injection wellhead pressure, bar
p_{wf} : bottom-hole injection pressure, bar
p_e : average reservoir pressure, bar
q : volumetric injection rate of water, m^3/d
q_m : mass injection rate of water, tons/h
Re : Reynolds number, dimensionless
r_e : external radius of the injected water front, m
r_{ci} : inner radius of cement, m
r_{co} : outer radius of cement, m
r_{pi} : inner radius of injection pipe, m
r_{po} : outer radius of injection pipe, m
r_w : wellbore radius, m
r_{wa} : apparent wellbore radius, m
S_{cd} : carbon dioxide gas saturation, fraction
S_w : reservoir water saturation, fraction
s : skin factor, dimensionless
TDS : total dissolved solids, ppm
T_i : temperature of injection water at any "z" and "t", °C
T_0 : wellhead temperature of injection water, °C
t : time, hours (or days)
U : overall heat transfer coefficient, W/m^2 °C/m
V_{cd} : volume of carbon dioxide at breakthrough, m^3
V_w : volume of reservoir water at breakthrough, m^3
W : cumulative water injection, m^3
z : depth, m

Greek Letters

α : thermal diffusion coefficient of earth, m^2/d
Δp_f : frictional pressure loss, bar
λ_c : thermal conductivity coefficient of cement, W/m °C
λ_e : thermal conductivity of earth, W/m °C
λ_p : thermal conductivity coefficient of pipe, W/m °C
μ_w : viscosity of water at injection temperature, mPa·s
μ_{rw} : viscosity of water at reservoir temperature, mPa·s
ρ : density of injected water, kg/dm^3
ρ_{rw} : density of reservoir water, kg/dm^3

REFERENCES

Altinay, E.I.: The Application of Hall Plot Method to the Injection Analysis in Geothermal Wells, *Graduation Study* (in Turkish), Petrol. and Natural Gas Eng. Dept. Istanbul Tech. Univ., Istanbul, Turkey, June (2002).

Buell, R., Kazemi, H., and Poettmann, F.H.: Analyzing Injectivity of Polymer Solutions with the Hall Plot, *SPE Reservoir Engineering*, 41-46, February (1990).

CRC: *Handbook of Chemistry and Physics*, 72nd edition, chief editor D. R. Lide, CRC Press, Inc., Ann Arbor, Michigan, U.S.A., 14-7 (1991)

Çengel, Y.A.: *Heat Transfer – A Practical Approach*, Int'l. edition, McGraw Hill Co. Inc., New York, New York, USA, (1998).

Earlougher, Jr., R.C.: *Advances in Well Test Analyses*, SPE Monograph Vol.5, Soc. of Pet. Eng., Dallas, TX, USA, 105-109, (1977).

Hall, H.N.: How to Analyze Waterflood Injection Well Performance, *World Oil* (Oct. 1963) 128-130.

Kasap, I.: Reinjection Test in Kizildere Geothermal Field, unpublished report (in Turkish), General Directorate of Mine Survey and Exploration, Ankara, Turkey (1976).

Ramey, H.J.: Wellbore Heat Transmission, *Journal of Pet. Tech.*, Soc. of Petrol. Eng., Richardson, Texas, USA, 427-435, April (1962).

Satman, A.: Solutions of Heat- and Fluid-Flow Problems in Naturally Fractured Reservoirs: Part 1 – Heat Flow Problems, *SPE Production Engineering*, Soc. of Pet. Eng., Richardson, Texas, USA, 463-466, Nov. (1988).

Satman, A., Serpen, U., Mihcakan, I.M.: Assessment of Reinjection Trials in Kizildere Geothermal Field, *Proceedings*, World Geothermal Congress, Kyushu – Tohoku, Japan, 1695-1700, June (2000).

Satman, A., and Ugur, Z.: Flashing Point Compressibility of Geothermal Fluids With Low CO_2 Content and Its Use in Estimating Reservoir Volume, *Geothermics*, 31, 29-44, Pergamon Press, Elsevier Sci. Ltd., (2002).

Steam Tables in SI Units - Wasserdampftafeln, 3rd enlarged edition, editors Grigull, U., Straub, J., and Schiebener, P., Springer-Verlag, Berlin, Germany (1990).

Tan, E.: Reservoir Characteristics of Kizildere Geothermal Energy Field, Restricted Report EP/SEM.9/R.34, Seminar on Utilization of Geothermal Energy for Electric Power Production and Space Heating, United Nations, Florence, Italy, 14-17 May (1984).

Ugur, Z..: Modeling of Calcium Carbonate Precipitation in Oil and Geothermal Fields, PhD Dissert. (in Turkish), Inst. of Sci. and Tech., Istanbul Tech. Univ., Istanbul, Turkey, 103-113, (1996).